Available at www.sciencedirect.com

ScienceDirect

journal homepage: www.elsevier.com/locate/he

Electrochemical performance of porous Ni_3Al electrodes for hydrogen evolution reaction

Hongxing Dong [a,b], *Ting Lei* [a], *Yuehui He* [a,*], *Nanping Xu* [c], *Baiyun Huang* [a], *C.T. Liu* [d]

[a] *State Key Laboratory for Powder Metallurgy, Central South University, Changsha, Hunan 410083, China*
[b] *Institute of Electro-Mechanical, Hangzhou Polytech, Hangzhou, Zhejiang 311402, China*
[c] *Membrane Science and Technology Research Center, Nanjing University of Technology, Nanjing 210009, China*
[d] *Department of Mechanical Engineering, The Hong Kong Polytechnic University, Hong Kong, China*

ARTICLE INFO

Article history:
Received 23 March 2011
Received in revised form
2 June 2011
Accepted 8 June 2011
Available online 18 July 2011

Keywords:
Porous Ni_3Al intermetallics
Reactive synthesis
Hydrogen evolution reaction
Electrocatalytic activity
Electrolysis

ABSTRACT

Porous Ni_3Al intermetallic material with a mean pore diameter of around 1 μm was prepared by step sintering Ni and Al powder pressed compacts in vacuum furnace at 900 °C. The electrocatalytic activity of the as-fabricated porous Ni_3Al material as an electrode for hydrogen evolution reaction (HER) in alkaline solutions was investigated by cyclic voltammetry (CV), linear sweep voltammetry (LSV) and electrochemical impedance spectroscopy (EIS) techniques. It is found that the onset potential of porous Ni_3Al for HER shifted in the positive direction favoring hydrogen generation with lower overpotential, compared with foam Ni and dense Ni electrodes. Effects of electrolyte concentration and temperature on HER as well as the electrochemical stability in alkaline solution were investigated and the electrochemical activation energy was determined for the porous Ni_3Al. The increased activity for HER was attributed to the high porosity, an increased electrochemical surface area and the nanostructure of porous Ni_3Al electrode. The corrosion tests showed that the corrosion resistance of porous Ni_3Al electrode changed during the immersion process due to the formation of passive film layers.

1. Introduction

Hydrogen, as a high-quality clean and renewable energy resource, is increasingly considered as one of the most promising candidates for the fuel of the future [1,2]. The production of hydrogen by water electrolysis is a simple, mature, large-scale industrial method, but the key problems of this technology mainly related to relatively low production rates and high energy consumption, restrain its commercial application at the present [3]. Optimizing structural design and developing advanced electrodes have been crucial to reduce the electrical consumption and improve the efficiency of water electrolysis [4,5]. Therefore, considerable research efforts have been conducted to enhance the electrocatalytic activity of electrodes to reduce the overpotentials for the hydrogen evolution reaction (HER) [6–9].

The increase of electrode surface area is one of the effective means of improving the activity of electrodes. Porous materials as electrodes for water electrolysis with larger surface area have been usually obtained through leaching active elements (such as Al, Zn, Cu, etc. [11–16]) out of the precursor, among which, porous Raney Ni [10] is a typical representative. However, the instability of Raney Ni limited its practical application due to the dissolution of active elements in working. Moreover, the electrocatalytic properties were reduced due to hydrogen bubble trapping in the small holes

* *Corresponding author*. Tel.: +86 731 88836144; fax: +86 731 88710855.
E-mail address: yuehui@mail.csu.edu.cn (Y. He).
0360-3199/$ – see front matter
doi:10.1016/j.ijhydene.2011.06.115

(usually <10 nm) during the HER process [4]. Therefore, in order to make water electrolysis more efficient and economical, there is a high demand to decrease the overpotentials of electrode reactions and to improve its catalytic performance as well as to select inexpensive electrode materials with good electrocatalytic activity.

Ni_3Al intermetallic compound has shown good alkaline corrosion resistance and special mechanical properties [17,18]. Therefore, it is possible for electrically conductive porous Ni_3Al materials to be used as electrodes in water electrolysis. In this paper, we presented a way to fabricate the novel porous Ni_3Al electrode by a combination of elemental reaction synthesis and step sintering process. The electrochemical behavior of hydrogen evolution and the electrocatalytic activity toward HER as well as the HER stability and corrosion behavior of the porous Ni_3Al electrode in alkaline solution were investigated.

2. Experimental

2.1. Preparation of porous Ni_3Al electrode

Commercially pure carbonyl Ni (3–5 μm) and gas atomizing Al (3–5 μm) powders were mixed in the ratio of Ni–14 wt%Al. The Ni and Al powders were ball-mixed for 10 h using a mixer, and pressed to compacts with a dimension of 5 mm × 45 mm × 1 mm under a pressure of 200 MPa. The specimens were then sintered in a vacuum furnace under 1×10^{-3} Pa at temperatures of 480, 580, and 900 °C for durations of 1 h followed by furnace cooling to room temperature. The heating rate was 2 °C min^{-1} during the whole process in order to avoid the possible self-propagating high-temperature synthesis (SHS) procedure and to realize near net-shape of porous Ni_3Al materials. The as-obtained porous Ni_3Al materials were examined by X-ray diffraction to identify the phase composition and corresponding crystalline structures.

2.2. Characterization of porous Ni_3Al

The morphology and composition as well as crystalline structures of the fabricated porous Ni_3Al were characterized by a field-emission scanning electron microscope (NOVA NANOSEM 230) equipped with EDX and X-ray diffractometry (XRD: D/MAX-255). The pore size distribution for porous Ni_3Al was measured by the mercury porosimeter method (Poremaster GT-60).

Electrochemical characterizations of porous Ni_3Al electrode for hydrogen evolution in 6 M KOH solution were carried out by cyclic voltammetry, cathodic polarization, and electrochemical impedance spectroscopy (EIS) techniques, respectively. The electrochemical measurements were carried out in a conventional three-electrode system, using 6 M KOH solution as electrolyte. The alkaline solutions were prepared with triple-distilled water. The working electrode was fixed in a Teflon holder, leaving a geometric surface area of 1 cm^2 exposed. The counter electrode was large Pt foil and the reference was a Hg/HgO electrode. All potentials are given vs the Hg/HgO electrode in 6 M KOH. The working electrode was reduced at −1.5 V for 600 s prior to each measurement.

Steady-state CV curves and Tafel curve were recorded in alkaline solution at a scan rate of 10 mV s^{-1} and 2 mV s^{-1}, respectively. The EIS measurements at different cathodic overpotentials were performed at the steady-state in the frequency range of 10 kHz to 0.1 Hz, and with the perturbation amplitude of 5 mV. For comparison, commercial foam Ni (porosity: 90%) and pure compact Ni electrodes were also tested.

3. Results and discussion

3.1. Morphology characterization of porous Ni_3Al

The scanning electron micrographs of porous Ni_3Al and green compacts are shown in Fig. 1. As could be seen in Fig. 1(a), the green compacts consist of Ni and Al particles. Fig. 1(b) shows the porous micrograph of the fabricated porous Ni_3Al, indicating a high open porosity up to 40%. The cross-section of sintered compact presented in Fig. 1(c) shows that the thickness of porous Ni_3Al is about 1 mm. Zooming in, a large number of interconnected pores are significant as shown by inset in Fig. 1(c). The pore formation mechanism during the elemental powder synthesis has been documented in other works [19].

Fig. 2 presents the typical pore size distribution diagram of porous Ni_3Al, indicating a relatively narrow pore size distribution with a mean pore diameter of around 1 μm. Furthermore, the electrical resistance measured by twin bridged technique is about 1×10^{-4} Ω cm, which resembles that of foam Ni (4.6×10^{-4} Ω cm), suggesting that the electrical conductivity of porous Ni_3Al is excellent.

3.2. XRD analyses of phase transformation during sintering process

The fabricated porous Ni_3Al was examined by X-ray diffraction to identify its phase composition and crystalline structure. Fig. 3 shows the XRD patterns of powder compacts at different temperatures. The green compact consists of only Ni and Al phases. As the temperature rises, peaks related to Ni_2Al_3 and Ni_3Al phases appear, while the Al peaks become weakened. The formation of intermediate phase during the sintering procedure results from the interdiffusion reaction between Ni and Al atoms in compacts. When the temperature reaches 900 °C, single Ni_3Al phase appears on the entire compact. Six peaks in the diffraction spectrum at 25°, 37.5°, 44°, 51°, 57.5° and 75° can be assigned to (100), (110), (111), (200), (210) and (220) planes of Ni_3Al, respectively. The grain size of Ni_3Al was estimated to be 14.9 nm, from the full width at half maximum of the most intense diffraction line of Ni_3Al (111) by Scherrer's equation [20].

3.3. Electrocatalytic evolution of hydrogen on porous Ni_3Al electrode

The electrocatalytic activity of porous Ni_3Al as an electrode for HER in alkaline solution was investigated. For comparison, foam Ni and bulk Ni electrodes are also measured. Cyclic voltammogram is employed to determine the double layer

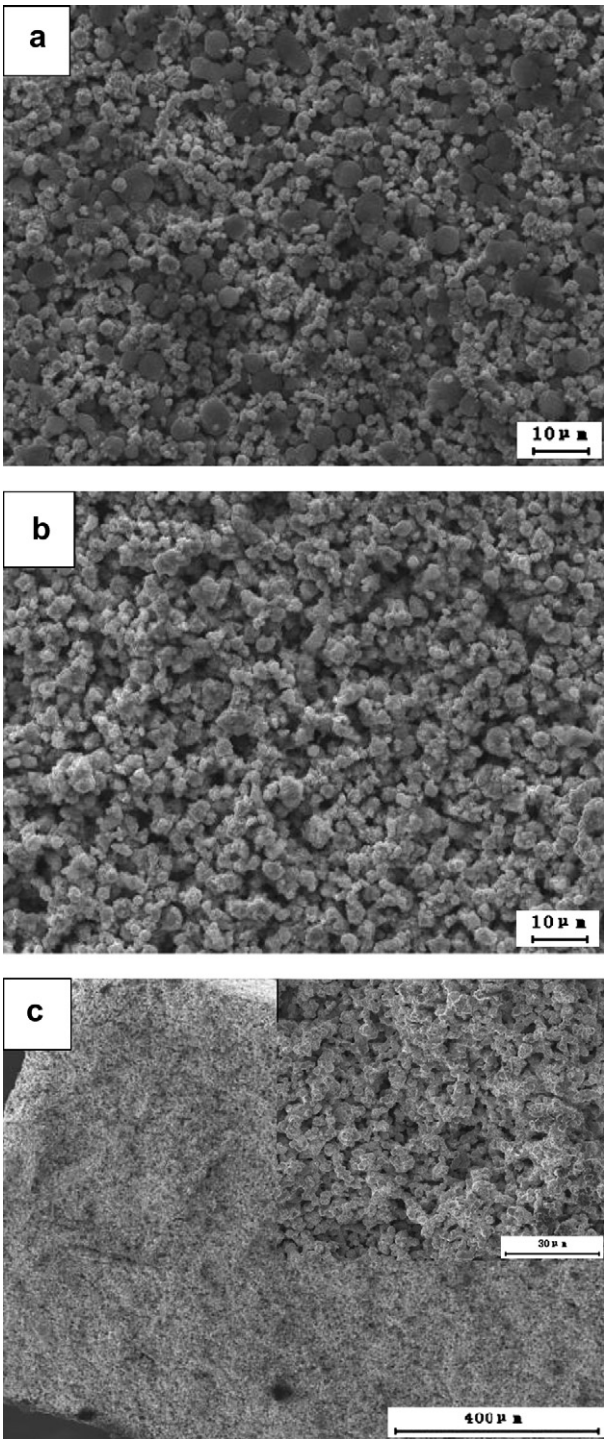

Fig. 1 – SEM morphology of porous Ni–Al: (a) green compacts; (b) sintered porous Ni–Al; (c) cross-section morphology, and the inset is a magnification of (c).

capacity of the porous Ni_3Al and the typical CV recorded at different sweep rates is displayed in Fig. 4(a). Stationary double layer currents are seen between the potential ranging from −0.28 to −0.18 V vs Hg/HgO. In this region, the average of capacitive current is proportional to the double layer capacitance, and the variation of the average of double layer current

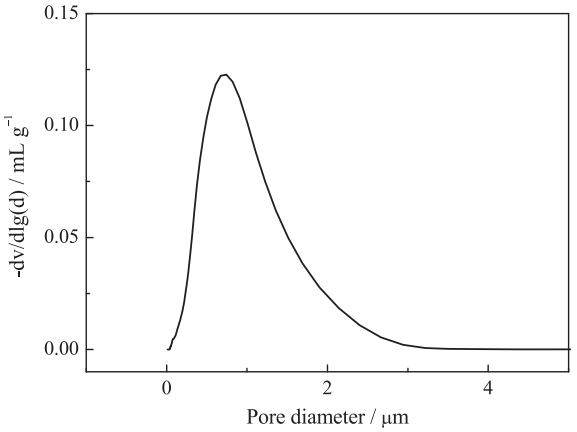

Fig. 2 – Pore distribution of porous Ni_3Al.

densities $j_{dl,ave} = (|j_c| + |j_a|)/2$ as a function of potential sweep rate is described as following [21]:

$$j_{dl,ave} = (|j_c| + |j_a|)/2 = C_{d1}\left(dE/dt\right) \quad (1)$$

where C_{d1} is the double layer capacitance of electrode, and j_c and j_a are cathodic and anodic current density, respectively. Plots of current density against sweep rate for all the three studied electrodes exhibit good linear relationship, as presented in Fig. 4(b). Therefore, the capacitances of three electrodes can be estimated from the slopes. The relative magnitude of the respective roughness factor, R_f, is calculated by assuming the value of 20 μF cm^{-2} for the capacitance of smooth mercury electrode, and the results are summarized in Table 1. The results indicate that both the capacitance order and roughness factor order are: porous Ni_3Al > foam Ni > bulk Ni, indicating that porous Ni_3Al has the largest active surface area.

The linear sweep cathodic polarization for HER in 6 M KOH is illustrated in Fig. 4(c). It shows that the cathodic current densities of the three electrodes increase as the overpotential increases. Moreover, the onset potential of porous Ni_3Al for

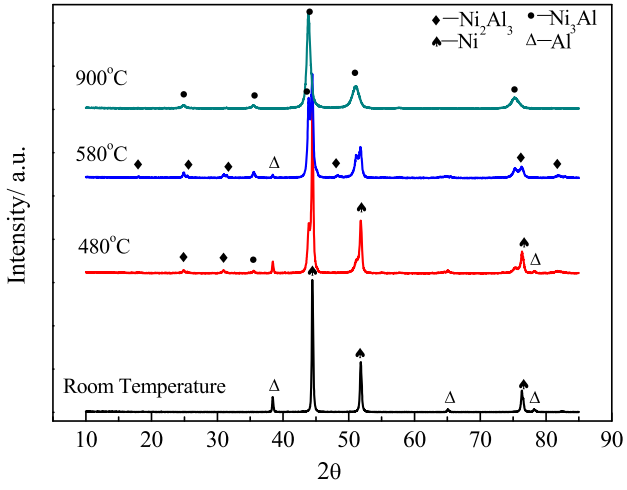

Fig. 3 – Phase transformation of porous Ni–Al during the sintering procedure.

HER is much more positive, favoring hydrogen generation with lower overpotential, as compared to foam Ni and pure compact Ni electrodes, which indicates that porous Ni_3Al has the higher hydrogen evolution activity and better electrocatalytic performance. The current density on porous Ni_3Al electrode is higher than 90 mA cm^{-2} at the potential of −1.35 V, which is 3 times higher than that on foam Ni electrode (26.9 mA cm^{-2}). The high electrocatalytic activity of the porous Ni_3Al electrode is likely attributed to the large electrochemical surface area.

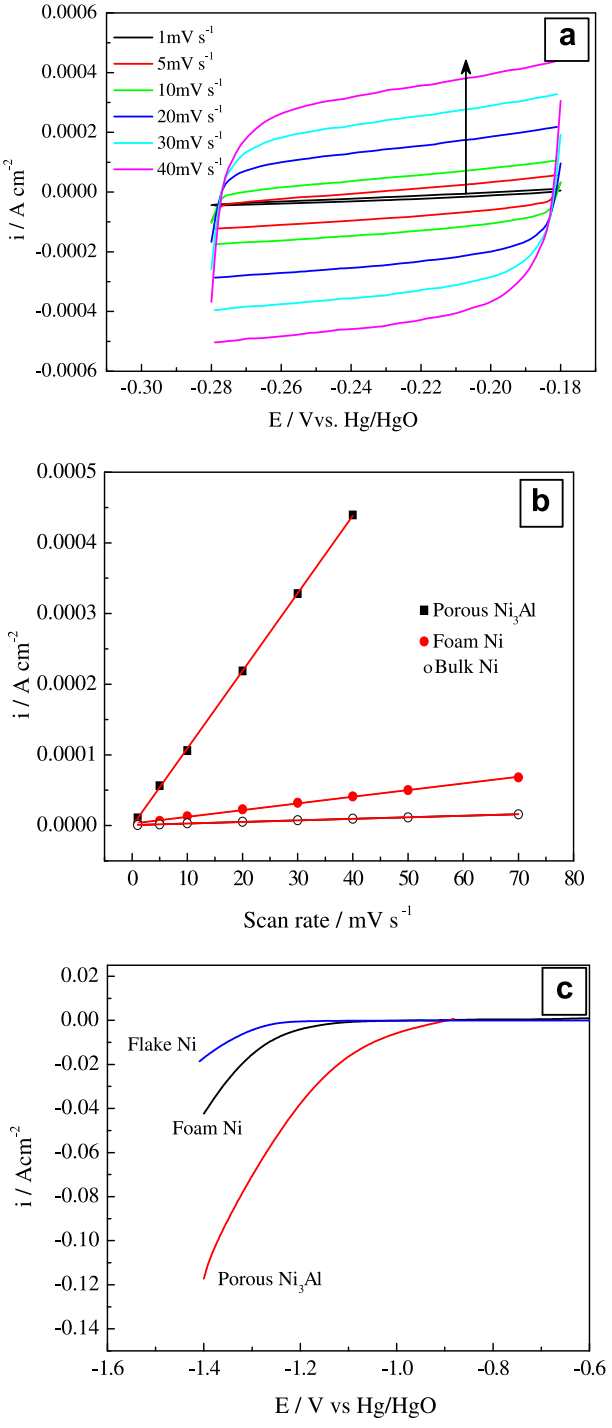

Fig. 4 – Electrochemistry properties of different cathode electrode: (a) cyclic voltammograms in the double layer region of the porous Ni–Al electrode at scan rates ranging from 1 to 40 mV s^{-1}; (b) mean current density as a function of scan rate for the electrodes; (c) the cathodic linear sweep for the electrodes at a scan rate of 10 mV s^{-1}.

Tafel slopes of the three electrodes for HER on the linear sweep curve at the lower overpotential region are summarized in Table 1. The exchange current density, j_0, a critical kinetic parameter in the dynamic electrochemistry, is derived directly from the intercept by the extrapolation of Tafel slope to equilibrium potential. As shown in Table 1, the Tafel slopes for porous Ni_3Al, foam Ni and pure compact Ni are 219, 130 and 107 mV, respectively. Generally, the lower Tafel slope indicates a favoring hydrogen generation. However, porous Ni_3Al exhibits a high Tafel slope. Interestingly, the increase of Tafel slope during HER has also been reported on other porous materials [22–25], the reason of which is likely due to the limit diffusion with respect to the complex and disordered porous structures [22]. Mathematical models also confirmed the high Tafel slope of porous materials during the HER process [26]. In addition, the exchange current density j_0 with respect to the effective electrode area is 3.4×10^{-3}, 6.15×10^{-4} and 5.9×10^{-4} mA cm^{-2} for porous Ni_3Al, foam Ni and pure compact Ni, respectively. Clearly, the j_0 on the porous Ni_3Al is 10 times larger, indicating that porous Ni_3Al has better catalytic properties for hydrogen evolution.

To further study the HER behavior on the interface of porous electrode and electrolyte, the electrochemical impedance spectra of porous Ni_3Al are recorded within the linear part of the potential region of Tafel plots, in which the steady-state conditions are ensured as shown in Fig. 4(c). The representative Nyquist plots of the porous Ni_3Al electrode at three different overpotentials are presented in Fig. 5. It shows that the entire complex plane plots displayed two depressed semicircles, where a small semicircle in the high frequency domains was almost independent of the potential, whereas the semicircle in the low frequency domain decreased with the increase in negative overpotential. Since the features in the complex impedance plane plots are consistent with that for the HER on porous electrodes in alkaline medium reported in literature [27,28], it is reasonable to suggest that the hydrogen evolution mechanism on porous Ni_3Al electrode is not modified during electrolysis and the hydrogen evolution should follow the same processes. Therefore, the high frequency semicircle was related to the electrode material and was independent of the kinetics of the faradic process, and the low frequency semicircle was attributed to the charge transfer resistance (R_{ct}) of the HER and was dependent on the kinetics of reaction. Consequently, the impedance data can be interpreted by an often used 2-CPE model containing a series connection of two parallel R-constant phase element (CPE) in series with uncompensated resistance due to the electrode configuration, which is well demonstrated in literature [5,29]. When the overpotentials increased, the R_{ct} decreased from 0.347 Ω cm^{-2} at $\eta = 75$ mV to 0.259 Ω cm^{-2} at $\eta = 135$ mV, indicating that R_{ct} is dependent on the overpotential (where the E_{equi} is 0.902 V vs Hg/HgO obtained from the experiment). On the other hand, the value of R_{ct} for porous Ni_3Al is lower than those of porous Ni electrode prepared by leaching Al out from Ni/Al and Ni/Zn precursors [26]. The lowest charge

Table 1 – Electrochemical properties of porous Ni_3Al electrode observed at potentials close to the limits of the studied domain.

Electrocatalysts	Tafel slope (mV/dec)	i_0 (mA/cm^2)	C_d (μF/cm^2)	R_f	i_0/S_{realf}[a] (mA/cm^2)	Onset potential (V vs Hg/HgO)	$I_{-1.35V}$ (mA/cm^2)
Pure flake Ni	107	0.007	234	11.7	5.9×10^{-4}	−1.25	10.1
Foam Ni	130	0.03	1007	50.4	6.15×10^{-4}	−1.15	26.9
Porous Ni_3Al	219	1.9	10,930	546.5	3.4×10^{-3}	−0.95	90.1

a Note: the exchange current of real surface area.

transfer resistance (R_{ct}) as well as highest value of the estimated exchange current density (j_0) confirms that the porous Ni_3Al electrode exhibits higher electrocatalytic activity toward hydrogen evolution than those foam Ni and pure compact Ni electrodes.

3.4. *Effect of parameters on the electrocatalytic properties*

3.4.1. *Effect of electrolyte concentration*

The effect of electrolyte concentration on HER is investigated and the results are illustrated in Fig. 6. Fig. 6(a) is the LSV curve recorded in KOH solution with concentrations ranging from 0.1 M to 8 M at a scan rate of 10 mV s^{-1}. Fig. 6(b) shows the variation of current density for HER as a function of KOH concentration (j–C) on porous Ni_3Al electrode at the potential of −1.3 V. The current densities increase with the increase of KOH concentration up to 6 M, and decrease thereafter. Apparently, porous Ni_3Al electrode exhibits the best electrocatalytic activity for HER in 6 M KOH solution.

It is generally accepted that the HER mechanism in alkaline solution is a combination of reaction steps involving the formation of adsorbed hydrogen [22,23]:

$$M + H_2O + e^- \underset{\leftarrow K_{-1}}{\overset{K_1}{\rightarrow}} MH_{ads} + OH^- \quad \text{(Volmer)} \tag{2}$$

$$MH_{ads} + H_2O + e^- \underset{\leftarrow K_{-2}}{\overset{K_2}{\rightarrow}} H_2 + M + OH^- \quad \text{(Heyrovsky)} \tag{3}$$

where the subscript ads represents the adsorbed status, k_i and k_{-i} ($i = 1, 2$) are the rate constants of the forward and backward reactions, which are influenced by the concentration of OH^- and H_2O. It is well known that an appropriate increase of the electrolyte concentration will increase solution conductivity and ion activity, which are advantageous to ionic transfer in the solution. During the HER process, H_2O and OH^- are competitively adsorbed on the electrode surface. When the electrolyte concentration is higher than 6 M, the increase of the concentration of electrolyte may result in an increase in the viscosity and a decrease in the ion activity, which in turn influences the departure of the bubbles and electron transfer.

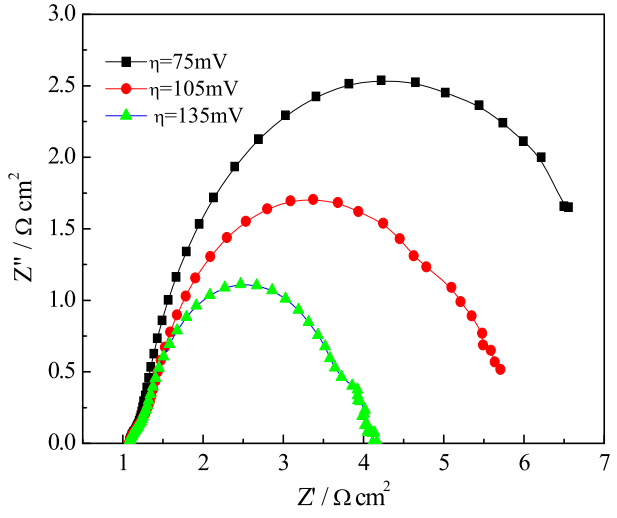

Fig. 5 – Nyquist plots for porous Ni_3Al electrode at different overpotentials.

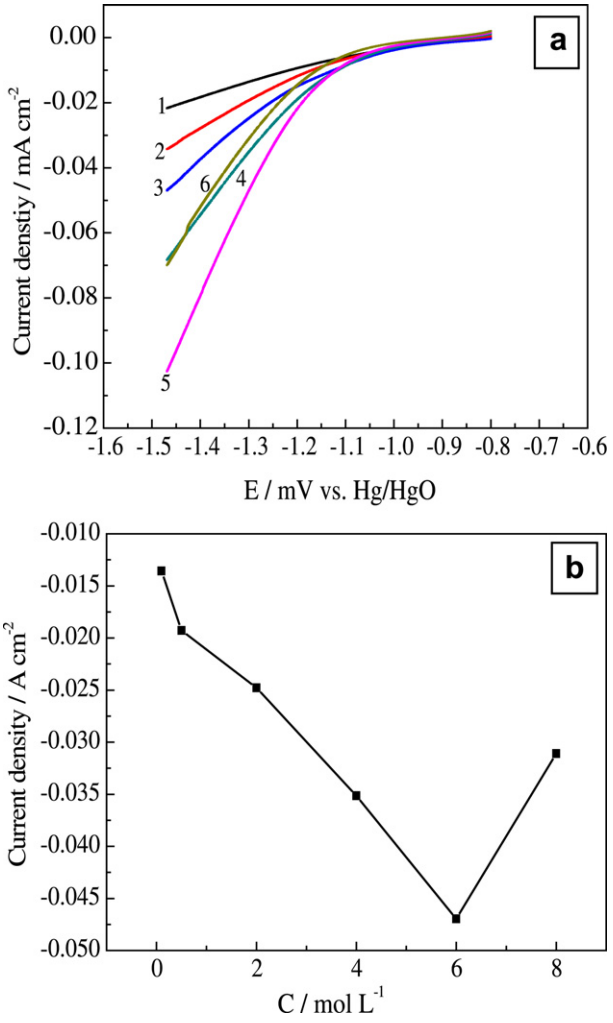

Fig. 6 – Influence of KOH concentration on the catalytic activity of porous Ni_3Al electrode for hydrogen evolution: 1: 0.1 mol L^{-1}; 2: 0.5 mol L^{-1}; 3: 2 mol L^{-1}; 4: 4 mol L^{-1}; 5: 6 mol L^{-1}; 6: 8 mol L^{-1}.

Meanwhile, higher concentration favors the adsorption of OH^- on the electrode surface, resulting in fewer sites for H_2O adsorption. As a result, the overall reaction rates for hydrogen evolution, corresponding to the forward reactions of Volmer and Heyrovsky steps, were reduced. Therefore, it is important to maintain a constant electrolyte concentration during the water electrolysis process.

3.4.2. *Effect of electrolyte temperature*

The Tafel plots recorded at different temperatures for the porous Ni_3Al electrodes are presented in Fig. 7(a). The inset in Fig. 7(a) indicates the linear part from which the kinetic parameters are derived. In order to ensure good reproducibility, the linear sweep voltammetry is swept from negative to positive potential direction. As could be seen in Fig. 7a, Tafel slope is very similar for all temperatures. However, the increase of temperature leads to a significant reduction of the overpotential and an increase of the exchange current density. For comparison, the HER behaviors are also characterized on foam Ni electrode at temperatures ranging from 25 to 55 °C, which displays the same increase trend with the increase of temperature. However, it is worthy to note that at temperature of 65 °C or higher, the foam Ni electrode exhibits decreased activity or even no activity for hydrogen evolution, and likely, serious passivation occurred on foam Ni at high temperature. Therefore, on this point of view, porous Ni_3Al shows relatively better stability for temperature.

From the cathodic polarization curves in 6 M KOH solution obtained at different temperatures, the exchange current densities are derived by extrapolation of Tafel slopes to zero overpotential, and the Arrhenius plot is present in Fig. 7(b). The curve of $\log j_0$ against T^{-1} exhibits a linear relationship and thus electrochemical activation energies for the HER could be calculated according to the following equation [30]:

$$\log j_0 = \log(FK_c) - \Delta G_0/2.303RT \quad (4)$$

where R is the gas constant and ΔG_0 is the apparent activation energy. The calculated value of apparent activation energy for porous Ni_3Al is 30.1 kJ mol^{-1}, lower than those obtained on Ni (35 kJ mol^{-1}), Ni–Mo–Cd (32 kJ mol^{-1}), Fe (39 kJ mol^{-1}), and Ni–Fe (31 kJ mol^{-1}) [31]. Apparently, porous Ni_3Al shows higher catalytic activity for HER by reducing the activation energy of the reaction, which is also confirmed by the reduced overpotential for hydrogen evolution as shown in Fig. 4(c). The

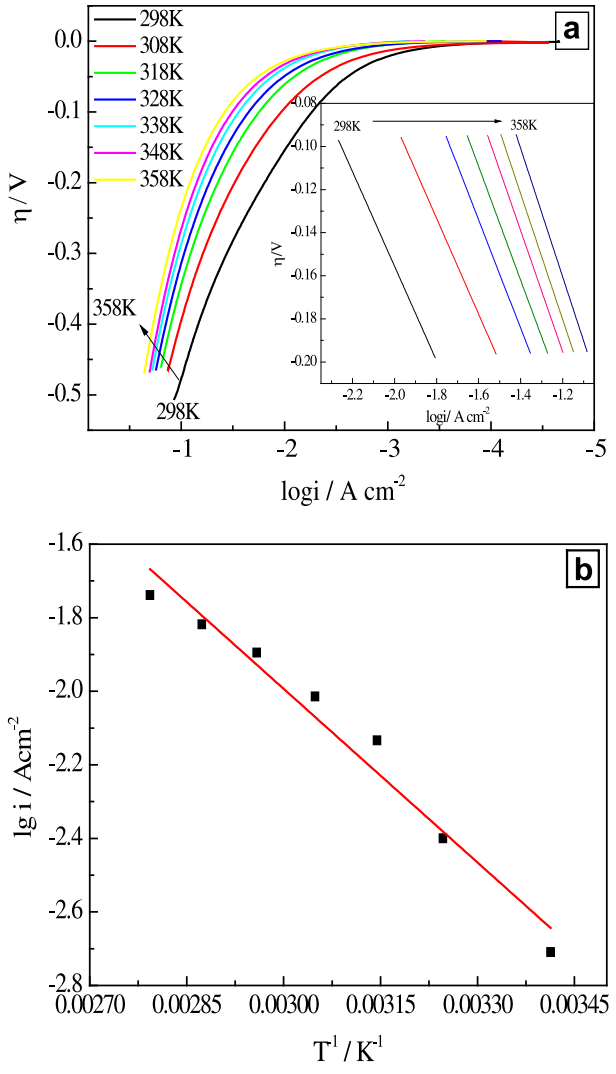

Fig. 7 – Influence of temperature on the catalytic activity of porous Ni_3Al electrode for hydrogen evolution.

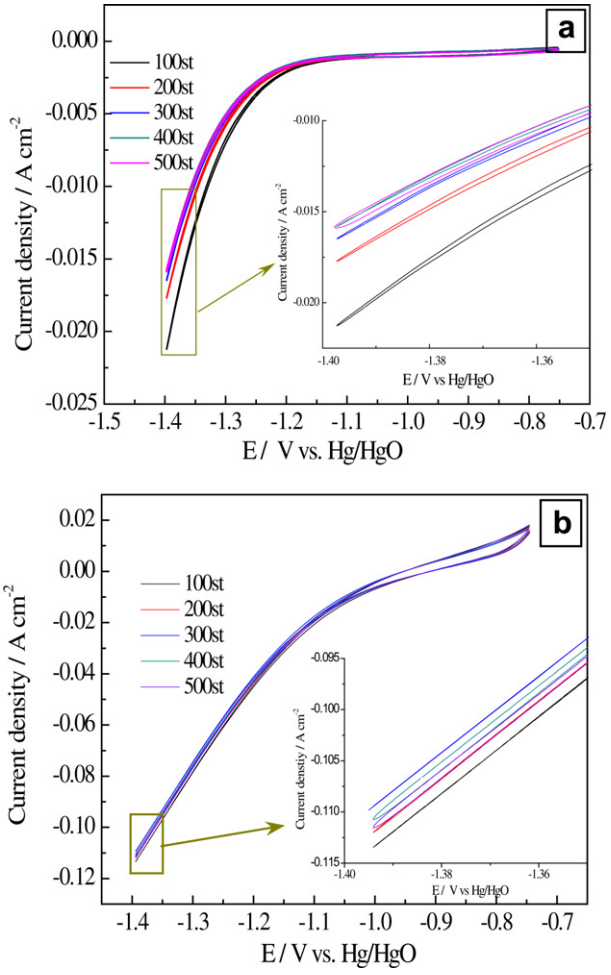

Fig. 8 – Cyclic voltammograms at a scan rate of 10 mV s^{-1} on porous electrodes in 6 mol L^{-1} KOH solution at different cycles: (a) foam Ni, (b) porous Ni_3Al.

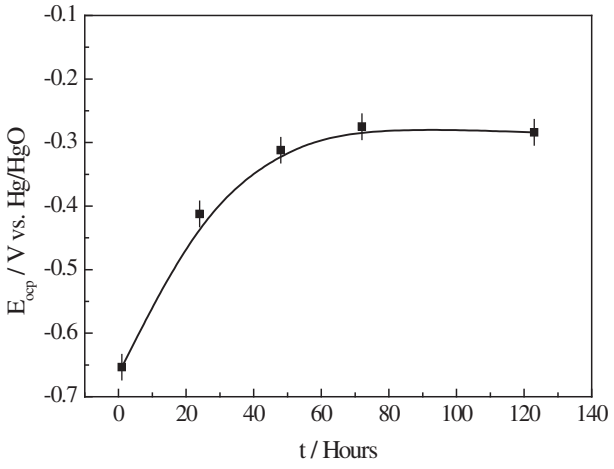

Fig. 9 – Change of open circuit potential with immersion time.

enhanced electrocatalytic activity of porous Ni_3Al is attributed to its specific characteristic and porous structure.

3.5. *The electrochemical stability of porous Ni_3Al*

The stability of porous electrode in alkaline solution is vital for its practical application. CV is employed to investigate the stability of porous Ni_3Al and foam Ni electrodes. Fig. 8 shows the cyclic voltammograms on foam Ni and porous Ni_3Al recorded in 6 M KOH solution at 298 K at a scan rate of 10 mV s^{-1} for 100–500 cycles in the potential range of −1.4 to −0.75 V. The hydrogen evolution current densities at −1.395 V for porous Ni_3Al at 100th, 200th, 300th, 400th, and 500th cycle are 113.8, 112.4, 109.8, 111.1 and 111.9 mA cm^{-2}, respectively. At the same potential, the hydrogen evolution current density for foam Ni at 100th, 200th, 300th, 400th and 500th cycle are 21.2, 17.7, 16.4, 15.7 and 15.9 mA cm^{-2}, respectively. Compared to the cathodic current density in the first cycle in alkaline solution shown in Fig. 3, the current decays for porous Ni_3Al after 100 and 500 cycles under the same conditions are about 1.6 and 7%, respectively, whereas the current decays for foam Ni after 100 and 500 cycles are 25 and 70%, respectively. It has also been reported a 37% current decay for foam Ni after 100 cycles in 6 M KOH among the potential region of −1.45 to −1.0 V [32]. These results suggest that porous Ni_3Al has higher electrochemical stability for hydrogen evolution than foam Ni.

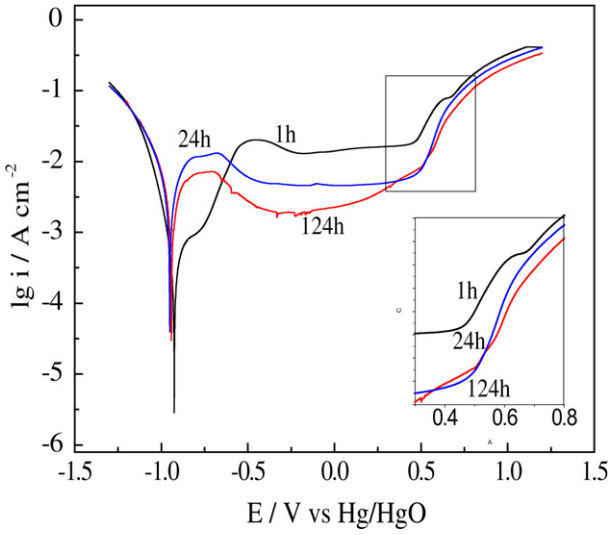

Fig. 10 – Tafel curves of porous Ni_3Al electrode after different exposure time in 6 mol L^{-1} KOH.

3.6. *The corrosion resistance of porous Ni_3Al*

The open circuit potential (E_{ocp}) of porous Ni_3Al electrode as a function of immersion time was also measured, which can give important results about porosity and corrosion behavior of metals [28]. The data obtained are given in Fig. 9. It shows that the E_{ocp} of porous Ni_3Al electrode started from an active value (−0.65 V) and shifted to a nobler direction with the immersion time, and then became stabilized after 50 h, indicating a good electrochemical stability. The change of the open circuit potential with time suggests the formation of passive film on porous Ni_3Al surface in alkaline solution.

Fig. 10 is the Tafel curves of porous Ni_3Al electrode after 1, 24 and 124 h exposure at open circuit conditions in 6 M KOH solution. It is speculated based on literature [11,33] that there probably exists NiO, NiOH and/or NiOOH between the potential range of −0.8 V to +0.5 V. Such a claim is supported by the results reported on NiCoZn electrode [28]. Furthermore, the anodic current densities decrease with increasing exposure time due to intensified surface passivity, indicating the better corrosion resistance of porous Ni_3Al in long-term immersion in alkaline solution. However, the cathodic current density of HER seems to be less influenced by the immersion time, implying an easy removal of any existing corrosion products from the porous Ni_3Al during hydrogen gas evolution. It also indicates that the formation of passive layer reduces oxygen evolution reaction (see Fig. 10 from +0.5 to +1.2 V).

The surface morphology and EDX analysis of porous Ni_3Al electrode after soaking in 6 M KOH solution for 124 h are displayed in Fig. 11. The EDX analysis suggested the formation of oxide or hydrated oxide on the porous Ni_3Al surface, which is in good agreement with the anodic passivation as depicted in

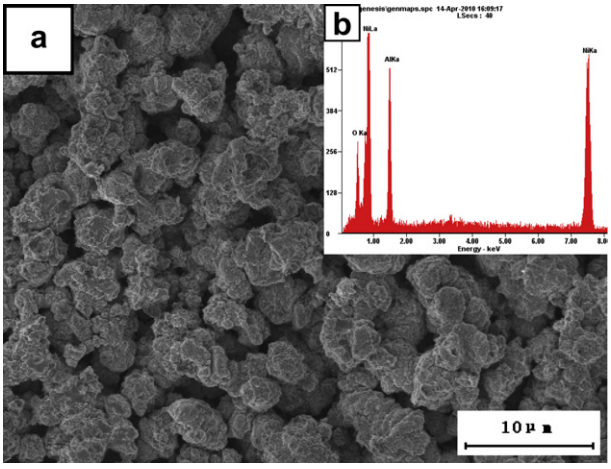

Fig. 11 – SEM micrograph and EDS analysis of porous Ni_3Al after 124 h exposure in 6 mol L^{-1} KOH.

Fig. 10. No significant changes are observed on the surface morphology of porous Ni_3Al after immersion in 6 M KOH solution in comparison with that of as-prepared porous Ni_3Al specimen shown in Fig. 1(b). Moreover, the ion concentration of Al and Ni in the alkaline solution after soaking for 124 h is about 4.32×10^{-6} g mL^{-1} and 1×10^{-8} g mL^{-1}, respectively, suggesting that the dissolution of Al and Ni is neglectable. Accordingly, the passive film may function as a barrier to improve the corrosion resistance of porous Ni_3Al in alkaline solution.

4. Conclusions

Ni_3Al intermetallic compound with porous structure was prepared through elemental powders reaction synthesis. The fabricated porous Ni_3Al had a narrow pore size distribution with a mean pore diameter of around 1 μm. The onset potential of hydrogen evolution on porous Ni_3Al is higher than that of foam Ni and dense Ni materials. The best catalytic performance was found for HER in 6 M alkaline solution. The apparent activation energy of porous Ni_3Al was 30.1 kJ mol^{-1}. Polarization measurements suggested that the formation of a passive film on porous Ni_3Al surface increased its corrosion resistance, but had little influence on its catalytic activity for the HER in alkaline medium. The excellent performance of hydrogen evolution of porous Ni_3Al may be ascribed to its specific characteristic and porous structure. Porous Ni_3Al exhibits better electrocatalytic activity toward hydrogen evolution reaction and electrochemical stability in alkaline solution, which is of important for practical application in water electrolysis for hydrogen generation.

Acknowledgments

This research was financially supported by the National Natural Science Foundation of China (No. 20476106, No. 50721003 and No. 20636020) and by the National Natural Science Funds for Distinguished Young Scholar (No. 50825102), “973” program (No. 2009B623400), “863” program (2006AA03Z511).

REFERENCES

[1] Ramachandran R, Raghu KM. An overview of industrial uses of hydrogen. International Journal of Hydrogen Energy 1998; 23(7):593–8.
[2] Armor JN. Catalysis and the hydrogen economy. Catalysis Letters 2005;101(3–4):131–5.
[3] Holladay JD, Hu J, King DL, Wang Y. Review: an overview of hydrogen production technologies. Catalysis Today 2009; 139(4):244–60.
[4] Marozzi CA, Chialvo AC. Development of electrode morphologies of interest in electrocatalysis: part 2: hydrogen evolution reaction on macroporous nickel electrodes. Electrochimica Acta 2001;46(6):861–6.
[5] Losiewicza B, Budnioka A, Rówińskia E, Giewkaa E, Lasia A. The structure, morphology and electrochemical impedance study of the hydrogen evolution reaction on the modified nickel electrodes. International Journal of Hydrogen Energy 2004;29(2):145–57.
[6] Kibria MF, Mridha MS, Khan AH. Electrochemical studies of a nickel electrode for the hydrogen evolution reaction. International Journal of Hydrogen Energy 1995;20(6):435–40.
[7] Zheng Haitao, Mathe Mkhulu. Hydrogen evolution reaction on single crystal WO_3/C nanoparticles supported on carbon in acid and alkaline solution. International Journal of Hydrogen Energy 2011;36(3):1960–4.
[8] Rosalbino F, Macciò D, Saccone A, Angelini E, Delfino S. Fe–Mo–R (R = rare earth metal) crystalline alloys as a cathode material for hydrogen evolution reaction in alkaline solution. International Journal of Hydrogen Energy 2011;36(3):1965–73.
[9] Adriana NC, Sergio ASM, Luis AA. Studies of the hydrogen evolution reaction on smooth Co and electrodeposited Ni–Co ultramicroelectrode. Electrochemistry Communications 1999;1(12):600–4.
[10] Tanaka S, Hirose N, Tanaki T. Evaluation of Raney-nickel cathodes prepared with aluminum powder and tin powder. International Journal of Hydrogen Energy 2000;25(5):481–5.
[11] Ramazan S, Gűféza K. Hydrogen evolution and corrosion performance of NiZn coatings. Energy Conversion and Management 2007;48(2):583–91.
[12] Chen LL, Andrzei L. Ni–Al Powder electrocatalyst for hydrogen evolution: effect of Heat-treatment on morphology, composition, and kinetics. Journal of the Electrochemical Society 1993;140(9):2464–72.
[13] Miao HJ, Piron DL. Composite-coating electrodes for hydrogen evolution reaction. Electrochimica Acta 1993;38(8):1079–85.
[14] Endoh E, Otouma H, Morimoto T. Advanced low hydrogen overvoltage cathode for chlor-alkali electrolysis cells. International Journal of Hydrogen Energy 1988;13(4):207–13.
[15] Xu CX, Wang LQ, Wang RY, Wang K, Zhang Y, Tian F, et al. Nanotubular mesoporous bimetallic nanostructures with enchanced electrocatalytic performance. Advanced Materials 2009;21(21):2165–9.
[16] Tanaka Sh, Hirose N, Tanaki T, Ogata YH. Effect of Ni–Al precursor alloy on the catalytic activity for a Raney-Ni cathode. Journal of the Electrochemical Society 2000;147(6): 2242–5.
[17] Wu L, Dong HX, He YH. Preparation and corrosion resistance in KOH solution of porous Ni_3Al. Chinese Journal of Materials Research 2011;25(2):118–23.
[18] Dong HX, He YH, Jiang Y, Wu L, Zou J, Xu NP, et al. Effect of Al content on porous Ni–Al alloys. Materials Science and Engineering A 2011;528(13–14):4849–55.
[19] He YH, Jiang Y, Xu NP, Zou J, Huang BY, Liu CT, et al. Fabrication of Ti–Al micro/nanometer-sized porous alloys through Kirkendall effect. Advanced Materials 2007;19(16): 2102–6.
[20] Crabb EM, Ravikumar MK. Synthesis and characterisation of carbonsupported PtGe electrocatalysts for CO oxidation. Electrochimica Acta 2001;46(7):1033–41.
[21] Bai C, Hong L, Li JB, Li X, Yang J, Tao J. Core-ring structured $NiCo_2O_4$ nanoplatelets: synthesis, characterization, and electrocatalytic applications. Advanced Functional Materials 2008;18(9):1440–7.
[22] Andrea K, Nicolae V, Waltraut B, Narcis D. Kinetics of hydrogen evolution reaction on skeleton nickel and nickel–titanium electrodes obtained by thermal arc spraying technique. International Journal of Hydrogen Energy 2007; 32(15):3258–65.
[23] Rami A, Lasia A. Kinetics of hydrogen evolution on Ni–Al alloy electrodes. Journal of Applied Electrochemistry 1992; 22(4):376–82.
[24] Lasia A. Hydrogen evolution/oxidation reactions on porous electrodes. Journal of Electroanalytical Chemistry 1998; 454(1):115–21.

[25] Los P, Rami A, Lasia A. Hydrogen evolution reaction on Ni–Al electrodes. Journal of Applied Electrochemistry 1993;23(2): 135–40.
[26] Hitz C, Lasia A. Experimental study and modeling of impedance of the her on porous Ni electrodes. Journal of Electroanalytical Chemistry 2001;500(1–2):213–22.
[27] Joël F, Danielle M, Legoux JG. Wire-arc sprayed nickel based coating for hydrogen evolution reaction in alkaline solutions. International Journal of Hydrogen Energy 1999;24(6):519–28.
[28] Solmaz R, Döner A, Şahin İ, Yuce AO, Kardas G, Yazici B, et al. The stability of NiCoZn electrocatalyst for hydrogen evolution activity in alkaline solution during long-term electrolysis. International Journal of Hydrogen Energy 2009; 34(19):7910–8.
[29] Jafarian M, Azizi O, Gobal F, Mahjani MG. Kinetics and electrocatalytic behavior of nanocrystalline CoNiFe alloy in hydrogen evolution reaction. International Journal of Hydrogen Energy 2007;32(12):1686–93.
[30] Zha QX. Introduction to electrode kinetics. Beijing: Science Press; 2002. p. 237.
[31] Carvalho JD, Tremiliosi-Filho GAL, Srinivasan AI, Wanger S, Wroblowa H. Electrode materials and processes for energy conversion and storage. Pennington: The Electrochemical Society; 1987. p. 356.
[32] Zheng HJ, Huang JG, Wang W, Ma CN. Preparation of nanocrystalline tungsten carbide thin film electrode and its electrocatalytic activity for hydrogen evolution. Electrochemistry Communications 2005;7(10):1045–9.
[33] Wang LP, Zhang JY, Gao Y, Xue QJ, Hua LT, Xu T. Grain size effect in corrosion behavior of electrodeposited nanocrystalline Ni coatings in alkaline solutions. Scripta Materialia 2006;55(7):657–60.